Hindawi
Advances in Civil Engineering
Volume 2022, Article ID 1991188, 12 pages
https://doi.org/10.1155/2022/1991188

Research Article

Effect of Joint Roughness and Infill Thickness on Shear Characteristics of Rock Mass

Xuezhen Wu,[1,2] **Hanfang Zheng**,[1] **Gang Wang**,[2] **Yuanjin Zhou**,[3] **and Zhenchang Guan**[1]

[1]*College of Civil Engineering, Fuzhou University, Fuzhou 350108, China*
[2]*Shandong Key Laboratory of Civil Engineering Disaster Prevention and Mitigation, Shandong University of Science and Technology, Qingdao 266590, China*
[3]*Binhai Airport Development and Construction Co., Ltd., Fuzhou 350108, China*

Correspondence should be addressed to Zhenchang Guan; gaussto@hotmail.com

Received 24 November 2021; Revised 21 December 2021; Accepted 11 January 2022; Published 31 January 2022

Academic Editor: Jian Xu

The joint planes in fractured rock mass will reduce the tensile strength and shear strength of rock mass, which has a decisive influence on the deformation and failure mode of engineering rock mass. Furthermore, infill also exists between the joint surfaces, which will also affect the shear characteristics of the joint. A method of importing standard joint profile into PFC2D was proposed, and a series of numerical simulation tests were carried out to study the effect of joint roughness and infill thickness on the shear characteristics of joints. The numerical results revealed that rock bolts profoundly improved the shear strength of the infilled rock joints, enhanced the toughness of the joint surface, increased the number of micro-cracks, and made the dilatation more obvious. The shear stress and the normal displacement of unbolted or bolted infilled rock joints increased with increasing the joint roughness and decreasing the infill thickness. The maximum horizontal compression stress in the middle of the bolt gradually increased with the increase of joint roughness coefficient. Different roughness has different effects on the number of micro-cracks in the sample. The number of total cracks and tensile cracks of the bolted and unbolted specimens increased with the increase of joint roughness coefficient, while the shear cracks remained almost the same. Through the study of the coupling effect of joint roughness and infill thickness on peak shear stress, results can be obtained as follows. The unbolted samples are highly sensitive to JRC changes. The greater the infill thickness, the greater the sensitivity of unbolted samples to JRC changes. The reinforcement effect of the bolt will strengthen the meshing strength between the joint surface and the filling material; that is, the meshing strength is positively correlated with joint roughness and negatively correlated with filling thickness.

1. Introduction

Rock mass is formed through long-term and complex geological processes; as discontinuous structural planes, joints are widely distributed in rock mass. The existence of joints will greatly reduce the strength of rock mass and increase the deformation of rock mass. A lot of engineering practice has proved that the failure of jointed rock mass is mainly the shear failure on the joint surface. Hence, the joint plane determines the strength and failure mode of rock mass to a great extent.

Many scholars have carried out research to study the influence of different factors on the shear characteristics of jointed rock mass, including joint inclination [1], joint roughness [2, 3], rock bridge [4, 5], shear rate [6], normal stress [7], friction coefficients [8], and temperature [9].

Due to the advantages of convenient processing and installation, high efficiency, and effective improvement of the strength and stability of jointed rock mass, bolt is widely used in geotechnical engineering to reinforce the rock mass [10]. In terms of laboratory tests, a series of shear tests were conducted to analyze the effect of friction angle along the joint, rock deformability, bolt inclination, joint dilatancy, normal stress, and bolt diameter on the improvement of joint shear resistance [11–16]. With the progress of technology, finite element method

(FEM) has been used to simulate the shear behavior of rock joints reinforced by rock bolts and their rupture behavior [17–20]. Saadat et al. [21] and Shang et al. [22] used discrete element simulation to study the shear behavior of bolted rock joints. They assumed that the bolt will not be damaged or deform during the shear process; the uniaxial compressive strength and Young's modulus of steel were much larger in compression compared to grout material. However, the bolt would be damaged by the shear load in the engineering practice. This caused the calculation results to be inconsistent with the actual results and exaggerated the role of the bolt.

According to Ren et al. [23], infilling can be found in natural rock joints which can affect the shear strength and failure mode of rock joints in practical engineering. Saadat et al. [21] proposed a new cohesive model to analyze the shear behavior of infilled rock joints. Gong et al. [24] investigated the variation of matric suction of joint infill during shearing and its influence on the shear behavior of irregular joints with compacted infill. Both unfilled and infilled rock joints are tested by taking into account the influences of initial normal stress, normal stiffness, and shear velocity [25].

In order to study the influence of joint roughness, filling thickness, and anchor structure on the shear characteristics of jointed rock mass, and the development law of microcracks, a method was proposed to digitize the standard joint profile and import them into numerical model, and a series of numerical simulation experiments were carried out.

2. Calibration and Establishment of Numerical Models

2.1. Calibration of Mesoscopic Parameters. Before the shear test, it is necessary to calibrate its calculated parameters, which must conform to the macroscopic characteristics of the rock mass. The parallel bonded model was calibrated against a uniaxial compression test on marble. A numerical specimen with a height of 100 mm and a width of 50 mm was produced as shown in Figure 1, and a calibration procedure was adopted to achieve the micro-properties. Notice that $R_{\min} = 0.25$ mm and $R_{\max}/R_{\min} = 1.66$ in PBM calibration, and it will be consistent with subsequent direct shear tests. Red and green lines in Figure 1 represent cracks generated after compression. The micro-parameters of the rock sample model in PFC are provided in Table 1. The stress-strain curves of the numerical simulation are shown in Figure 2. The results showed that the uniaxial compressive strength, Young's modulus, and Poisson's ratio of the model were 155.64 MPa, 53.63 GPa, and 0.20, respectively. Poisson's ratio is defined by the following calculation. When the specimen reaches 50% compressive strength, the axial strain and horizontal strain of the specimen were recorded, and Poisson's ratio was calculated according to the following formula.

$$\nu = \left| \frac{\varepsilon_{2(50)}}{\varepsilon_{1(50)}} \right|, \tag{1}$$

where $\varepsilon_{1(50)}$ is the axial strain corresponding to $(\sigma_1 - \sigma_3)_{50}$ and $\varepsilon_{2(50)}$ is the horizontal strain corresponding to $(\sigma_1 - \sigma_3)_{50}$.

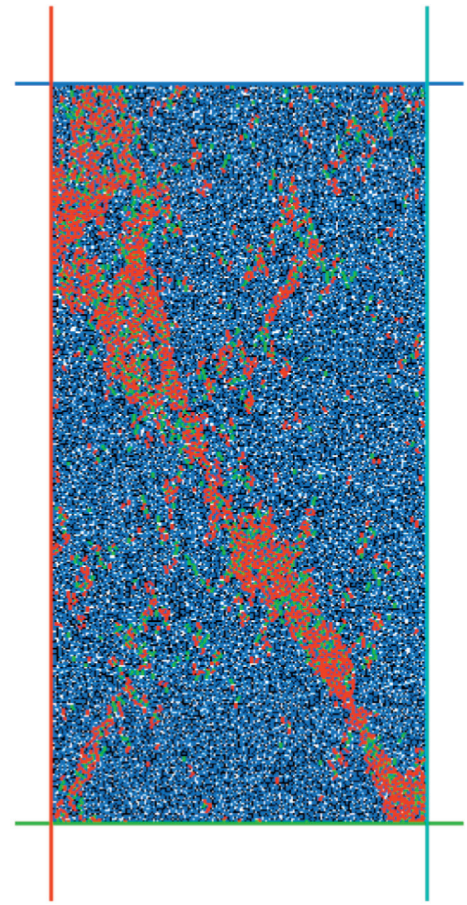

Figure 1: Numerical model for calibration.

The comparison between mechanical parameters of the numerical and physical specimens is shown in Table 2. The mechanical parameters obtained in the laboratory test [26] are similar to those obtained in the numerical simulation test. Hence, the micro-mechanical parameters given in Table 1 can be applied to the shear test of anchoring filling joints.

2.2. Setup of 2D Direct Shear Tests of Bolted Infilled Rock Joints. The established numerical model of bolting jointed rock mass is shown in Figure 3. The constructed digital elevation model (DEM) sample has a length of 100 mm and a height of 50 mm, which consist of around 11,686 particles with minimum particle radius $R_{\min} = 0.25$ mm and $R_{\max}/R_{\min} = 1.66$ that follows a uniform distribution. Two additional walls (Wall 7 and Wall 8) were created to prevent particles from overflowing during shearing. To generate the numerical specimen, the particles were divided into four different groups: rock, infilled rock joints, grout, and rock bolt. The particles of rock are shown in blue color; the particles of infilled rock joints are shown in yellow color; the particles of grout are shown in green color; and the particles of rock bolt are shown in red color. In practical engineering, rock bolts with a diameter of 20 mm are generally considered to be arranged at a distance of 1 m. The length of the numerical model is 0.1 mm; therefore, the diameter of the bolt

Table 1: The calibrated micro-mechanical parameters of marble.

Micro-properties	Particle density ($kg \cdot m^{-3}$)	Particle modulus (GPa)	Particle normal to shear stiffness ratio	Parallel bond modulus (GPa)	Parallel bond normal to shear stiffness ratio	Parallel bond cohesion (MPa)	Parallel bond tensile strength (MPa)
Values	2500	32	1.6	32	1.6	58	58

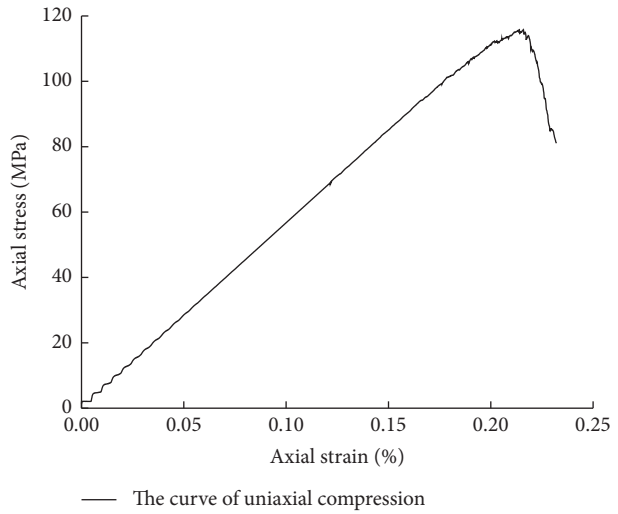

Figure 2: The curve of uniaxial compression.

Table 2: Mechanical parameters of marble.

Mechanical parameters	Compressive strength (MPa)	Young's modulus (GPa)	Poisson's ratio
Experimental	115.73	53.78	0.21
Numerical	115.64	53.63	0.20

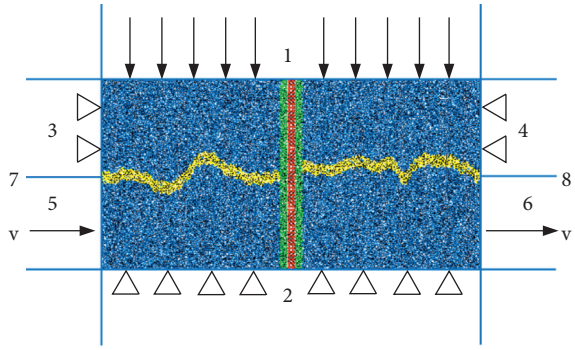

Figure 3: Schematic diagram of shear numerical model.

in PFC was also scaled down. We set a diameter of 2 mm for the rock bolt and a thickness of 4 mm for the grout.

The standard curve of joint roughness suggested by Barton and Choubey [27] was digitized and used to produce rock joints. The steps are as follows: Firstly, we scaled the standard joint contour according to the size of the numerical model to be built. Then, the different standard contour lines were divided into 100 short segments in CAD as shown in Figure 4, and the coordinate values of the two endpoints of each segment were obtained. For the model without

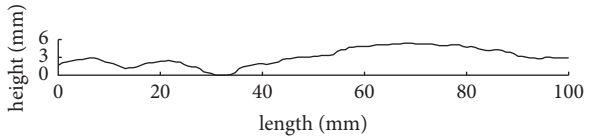

Figure 4: Schematic diagram of standard joint contour line division.

considering the fillings, only one contour line needs to be imported. We entered the endpoint coordinates into the command stream file when building the model in PFC. We connected all short segments in turn to form a complete contour line of the standard joint contour, that is, the boundary of particles. For the model considering the fillings, it is necessary to input the upper and lower contour lines in turn, and we considered these to be parallel lines. The input method is similar to the above, but there is a difference in the Y coordinate value (along the direction of specimen height) of each pair of parallel line segments of the upper and lower contour lines; this difference is the filling thickness to be set. When the particles were generated in the following steps, the particles located between the upper and lower contours were defined as fillings. Hence, a numerical model of joints with fillings was established.

In the test model, the particle size of the rock, infilled rock joints, and grout groups are set to be the same. The bolt adopts a parallel bonding constitutive model, which is composed of 100 red particles separated from each other. When it is bonded, it resists torque and behaves as linear elasticity. If their strength is exceeded, the parallel bond can be broken, and they cannot transmit force and moment. Figure 5 illustrates the force-displacement law of parallel

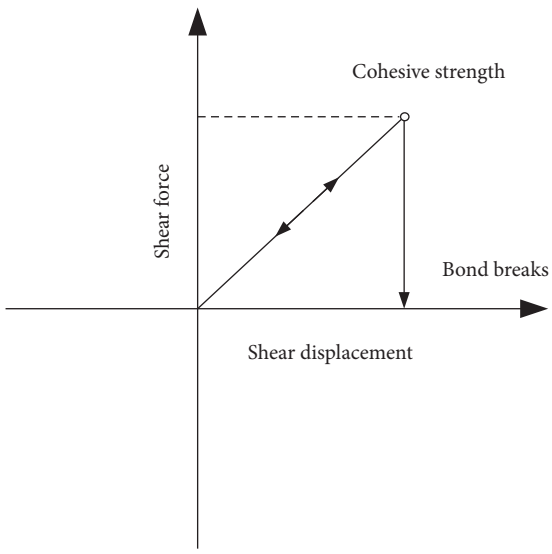

Figure 5: Shear force-shear displacement law of the PBM.

bond model (PBM) under shear loading. It can be observed that when a contact reaches its yielding limit (cohesive strength), the contact forces will abruptly reduce to zero.

A direct shear test under constant normal stress of 4 MPa was carried out. The normal load was applied vertically to the upper block, and this load was kept constant during the test by using a servo-control mechanism. In the shear process, the upper box was fixed, and the lower box was sheared in the positive X direction at a constant velocity of 0.2 m/s to ensure quasi-static equilibrium. Calculations in PFC are based on an explicit time-stepping algorithm. Because the calculation in the particle discrete element is based on the explicit time-stepping algorithm, the time step of each calculation is 2.76×10^{-8} s under the condition that the shear speed is 0.2 m/s. This means that the lower shear box is moving horizontally to the right at a rate of 1.38×10^{-9} m/step. At this point, the shear rate of the sample is slow enough to ensure the quasi-static equilibrium of the sample in the shear process.

The horizontal displacement of Wall 5 was used to calculate shear displacement during shearing. The displacement of the top wall in the normal direction was measured at each time step to produce the normal displacement of the rock joint. The average shear stress is the ratio of the average value of the reaction force on the two side walls of the upper and lower boxes to the area of the initial joint surface. The shearing was terminated when the shear displacement of the specimen reached the preset value of 1 mm, and the shear stress, normal displacement, and the number of microscopic cracks of the specimen were dynamically recorded during the shearing process.

3. Effect of Joint Roughness and Infill Thickness

3.1. Effect of Joint Roughness on Shear Characteristics. In order to determine the influence of joint roughness, three types of rock joint sections with different joint roughness coefficients (JRC 6–8, JRC 12–14, and JRC 18–20) were subjected to direct shear tests. The longitudinal section of these infilled rock joints is shown in Figure 6. The spacing between the upper and lower contour lines is 2.1 mm; that is, the thickness of joint infill is 2.1 mm. Six groups of shear mechanical tests of bolted and unbolted joints were carried out under three different joint roughness coefficients.

Figure 7 illustrates the relationship between shear stress and shear displacement of infilled rock joints model under different joint roughness. Figure 8 clearly shows the simulation results with those obtained for bolted and unbolted infilled rock joints under different joint roughness coefficient conditions. The numerical simulation results are similar to the indoor test conducted by Wu et al. [28]. The observation was that the peak shear stresses for JRC 6–8, JRC 12–14, and JRC 18–20 were 9.39 MPa, 10.75 MPa, and 13.67 MPa, respectively, under bolted infilled rock joints. For unbolted cases, the peak shear stresses were 4.24 MPa, 7.55 MPa, and 11.17 MPa, respectively. It is also noted that the bolt improved the peak shear stress of the infilled joint. The values of the increase in peak shear stress for JRC 6–8, JRC 12–14, and JRC 18–20 were 5.15 MPa, 3.20 MPa, and 2.50 MPa, respectively. It can be seen that the impact of the bolt on the shear stress during the shearing process is as follows:

(1) It is noted that at the initial stage of the shear test, the shear stress curve of bolted infilled rock joints was similar to that of the unbolted cases. It was elastic stage at the beginning of shearing, and the shear stress increases rapidly.

(2) After the shear stress of the unbolted infilled rock joints reached its peak value, it decreased and eventually stabilized. As for the bolted infilled rock joints, the sudden drop in shear stress represents bolt fracture. Then, the shear stress tends to be the sample without bolt. The shear stress of the bolted rock joints has a larger shear displacement before reaching the peak.

(3) Regardless of whether the infilled rock joints are bolted or not, the shear stress increases as the joint roughness coefficient increases, and the peak shear stress of bolted infilled rock joints was higher than unbolted cases.

Dilatancy is the phenomenon that the upper block is lifted upward with the development of shear displacement during the shearing of the specimen along the shear plane. Figure 9 shows that the bolted and unbolted infilled rock joints produced the same dilation behavior at different joint roughness coefficients. The numerical test results of the relationship between shear displacement and normal displacement were similar to the research results [29]. Normal displacement increased with increasing joint roughness coefficient. The normal displacement of the bolted specimens was greater than that of the unbolted specimens. At a shear displacement of 1.0 mm for unbolted cases, the normal displacements for the three JRC cases were 0.195 mm, 0.271 mm, and 0.334 mm, respectively. When the infilled rock joints were reinforced by rock bolts, they had a high

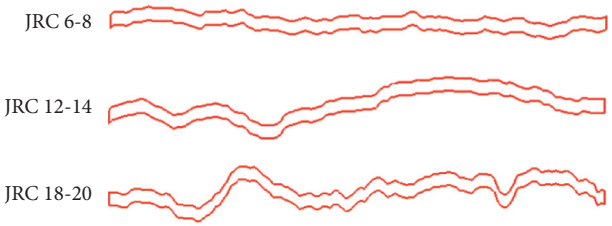

Figure 6: Schematic of discontinuities with 3 different roughness coefficients.

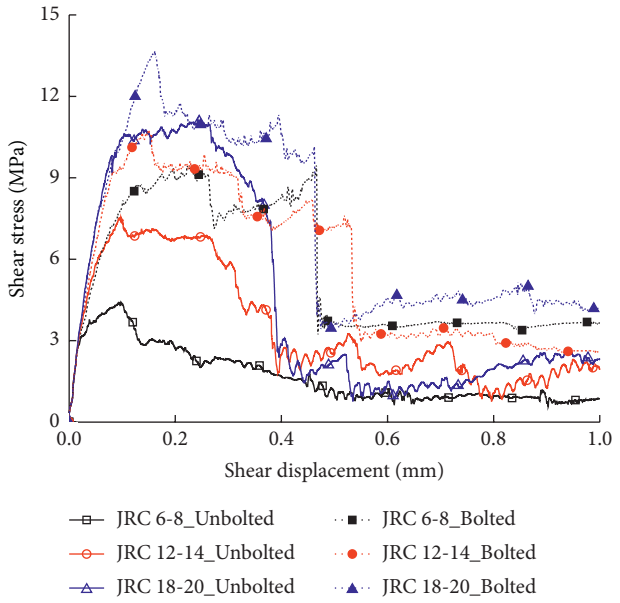

Figure 7: Relationship between shear stress and shear displacement under different joint roughness.

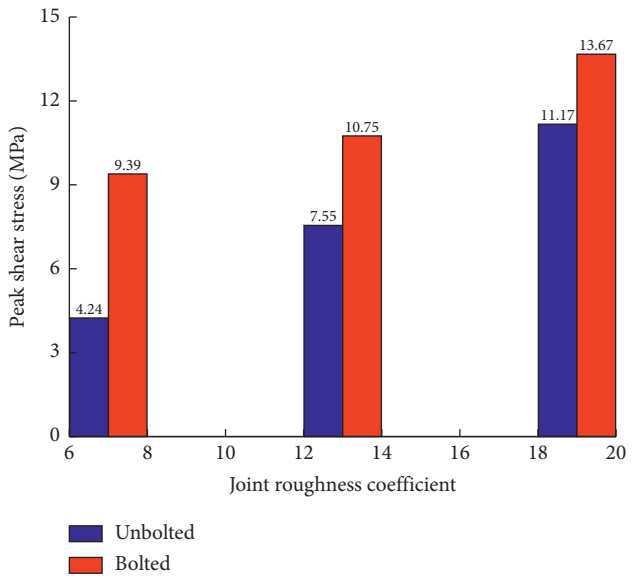

Figure 8: Relationship between peak shear stress and joint roughness coefficients.

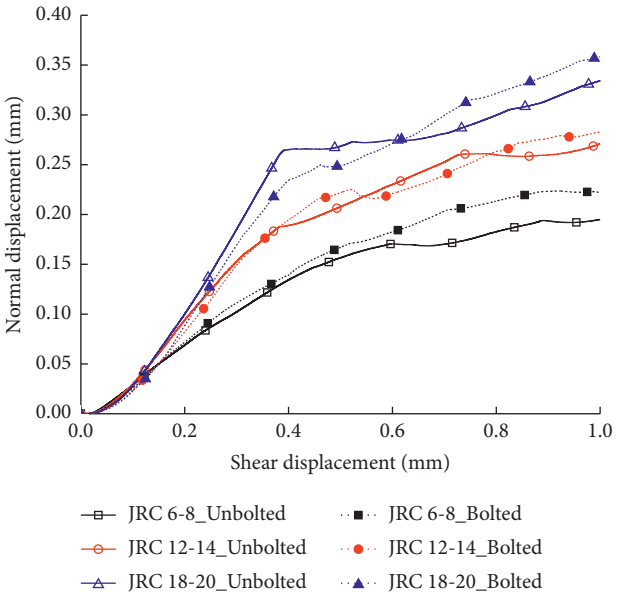

Figure 9: Relationship between normal displacement and shear displacement under different joint roughness.

shear resistance which led to a greater normal displacement. The total normal displacements for the three cases were 0.222 mm, 0.282 mm, and 0.358 mm, respectively under bolted infilled rock joints.

As shown in Figure 10, five measurement circles were uniformly distributed in the rock bolt to study the evolution process of the stress on the bolt in the direct shear tests. The radius of the five measurement circles was consistent with the radius of the bolt. The force diagram of the cell cube of measurement circles is illustrated in Figure 11. The evolution of horizontal compressive stress S_{xx}, shear stress S_{xy}, and normal compressive stress S_{yy} could be monitored by measurement circles.

The shear performance of bolted infilled rock joints with an infill thickness of 2.1 mm and JRC 18–20 was studied to understand the evolution of the stress on the bolt. The maximum stress distribution which was monitored by measurement circles on the bolt as shown in Figure 12. During the shearing process, the stress on the bolt was uniformly distributed. The horizontal compressive stress S_{xx}, shear stress S_{xy}, and normal compressive stress S_{yy} at the intersection of the bolt and the joint were higher than those in other positions. The joint roughness coefficient has an important influence on the distribution of maximum horizontal compressive stress. As shown in Figure 13, the maximum horizontal compression stress in the middle of the bolt gradually increased with the increase of JRC.

3.2. Effect of Joint Roughness on Micro-Cracks. Different roughness has different effects on the number of micro-cracks in the sample. The relationship between the number of micro-cracks and the joint roughness coefficient is shown in Figure 14. The number of total cracks and tensile cracks of the bolted and unbolted specimens increased with the increase of joint roughness coefficient, while the shear cracks

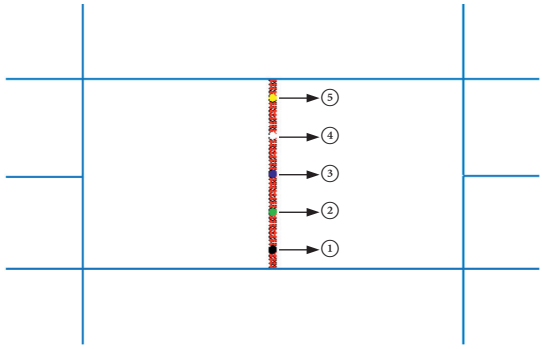

Figure 10: Position of measurement cycle.

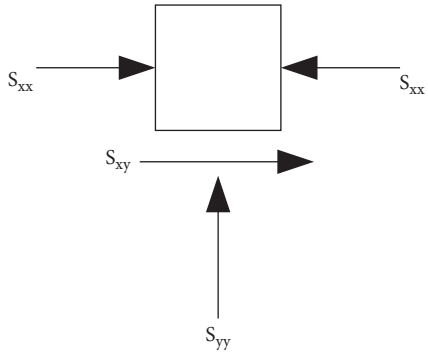

Figure 11: Force diagram of cell cube.

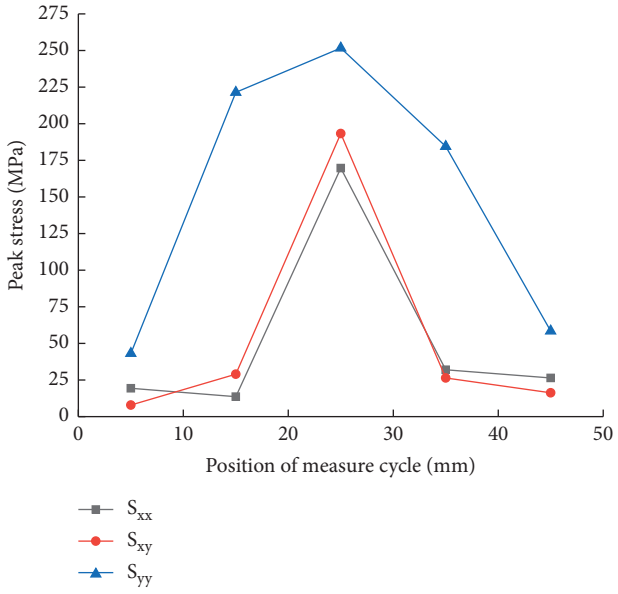

Figure 12: Distribution curves of stress on the bolt.

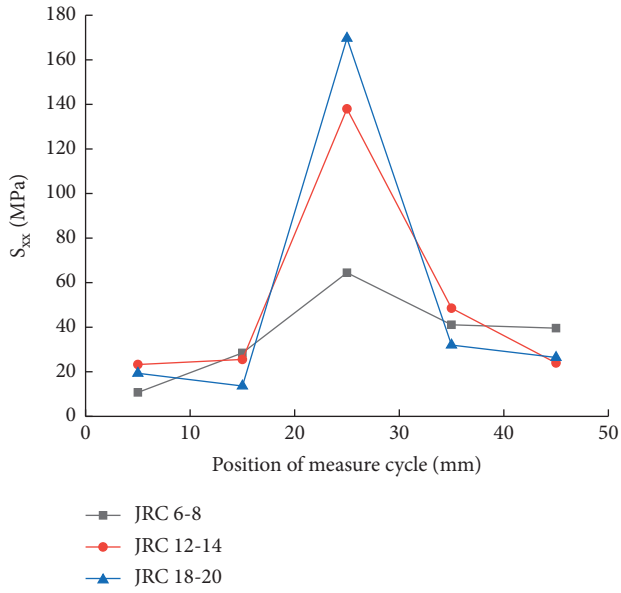

Figure 13: Distribution curves of S_{xx} on the bolt.

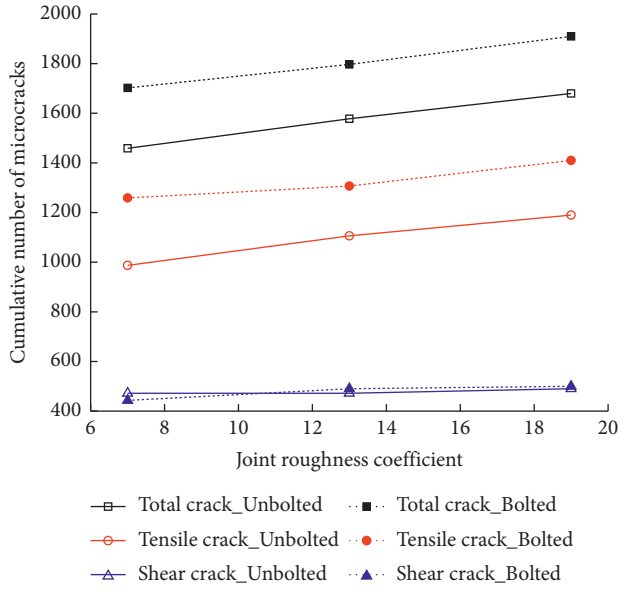

Figure 14: Relationship between JRC and micro-cracks.

remain almost the same. The crack development diagram of JRC 18–20 with an infill thickness of 2.1 mm is shown in Figure 15; they were dominated by tension cracks. For the bolted cases, the number of tensile micro-cracks was 1490 which was around 2.98 times that of shear micro-cracks (500). The development curve of the number of cracks could be divided into three stages. At the first stage, there were a few micro-cracks in the sample at the beginning of the shear test. When the shear stress increased to a certain strength, micro-cracks began to gradually increase. At the second stage, the number of micro-cracks increased with increasing shear displacement. When the shear stress reached the peak strength, the growth rate of the number of cracks increased rapidly. At the third stage, the growth rate of cracks gradually smoothed out, and eventually the number of cracks tended to be constant.

The evolution process of micro-cracks is graphically illustrated in Figures 16 and 17. Shear cracks were shown in green and tensile cracks in red. Modes of bolted and unbolted specimens were different during the shearing process. When the shear displacement was 0.01 mm, 0.02 mm, 0.05 mm, 0.1 mm, 0.5 mm, and 1.0 mm, the

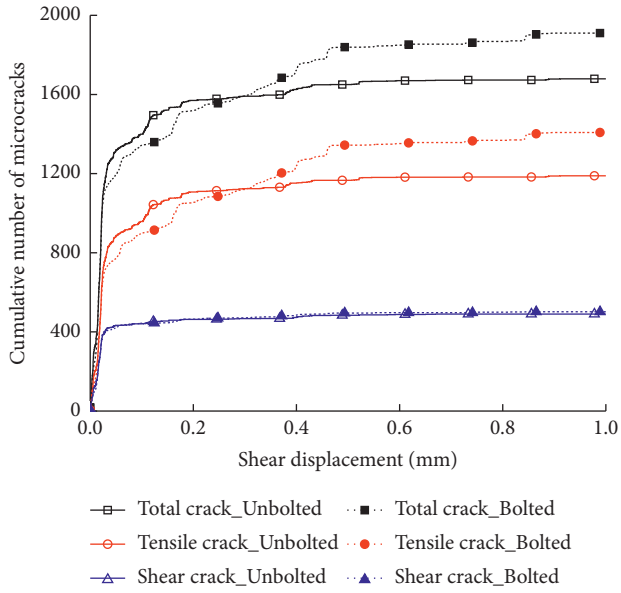

Figure 15: Relationship between shear displacement and micro-cracks.

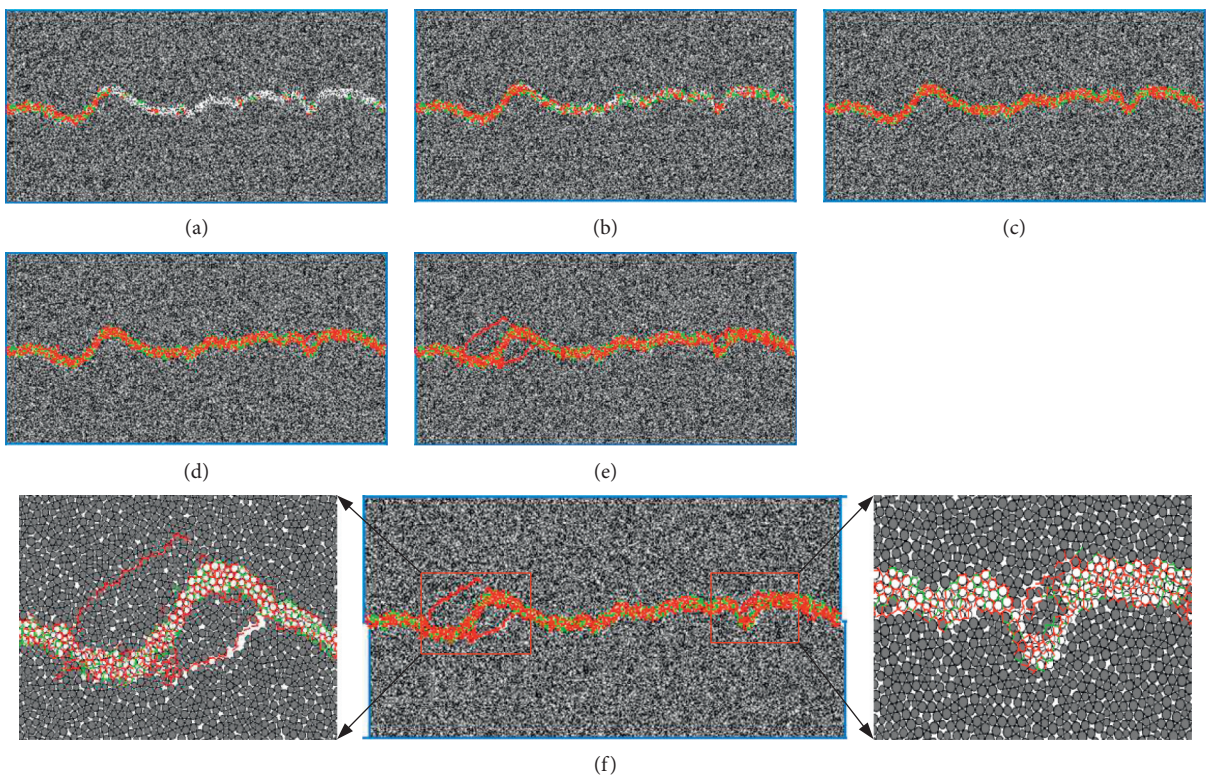

Figure 16: The development of micro-cracks of unbolted infilled rock joints: (a) 0.01 mm; (b) 0.02 mm; (c) 0.05 mm; (d) 0.1 mm; (e) 0.5 mm; (f) 1.0 mm.

crack development of bolted and unbolted specimens were recorded.

For the unbolted infilled rock joints, it can be observed that cracks began to form around the head of rock joints (see Figure 16(a)). As the shear displacement of the specimen increased, the cracks of the infill at the joint continued to increase (see Figure 16(b)). When the shear displacement was 0.05 mm, the infill has been completely penetrated by cracks (see Figure 16(c)). As shown in Figure 16(d), micro-cracks appeared around the joint. When the shear displacement reached 0.5 mm, the micro-cracks around the joint gradually increased (see Figure 16(e)). When the shear

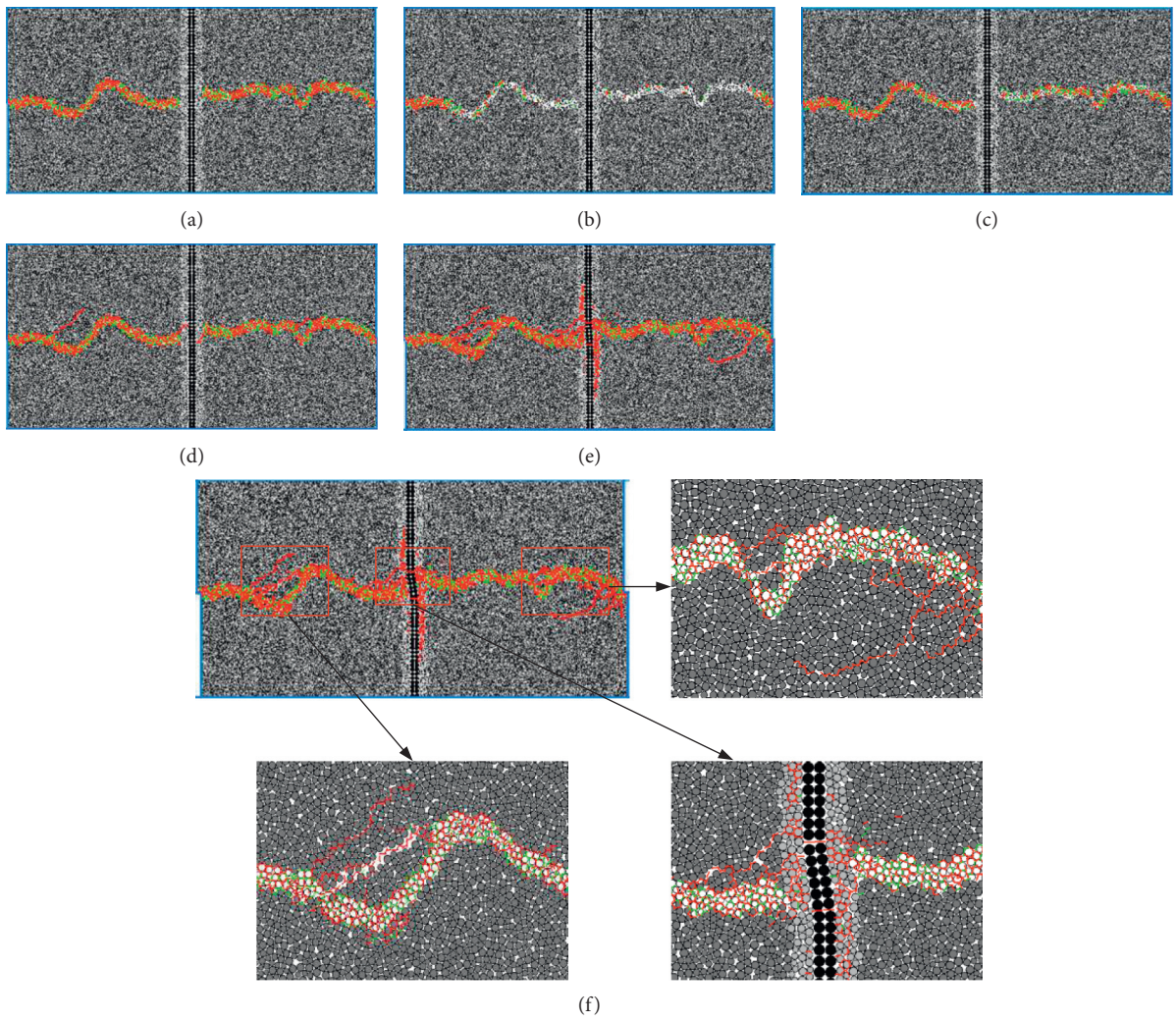

Figure 17: The development of micro-cracks of bolted infilled rock joints: (a) 0.01 mm; (b) 0.02 mm; (c) 0.05 mm; (d) 0.1 mm; (e) 0.5 mm; (f) 1.0 mm.

displacement reached 1 mm, the shearing process of the unbolted specimen finished as shown in Figure 16(f). There were many cracks at the joints with steeper asperity angles. Another observation was that the number of tensile cracks was significantly higher than that of shear cracks.

During the shearing of the bolted infilled rock joints, it can be observed that cracks began to form around two edges of rock joints (see Figure 17(a)). As the shear displacement of the specimen increased, the development trend of the crack was similar to the unbolted specimen. The crack first extended at the infilled rock joints and was then generated at the intersection of the joint and the rock (see Figures 17(b)–17(d)). When the shear displacement was 0.5 mm, the bolt was destroyed, and a lot of cracks were generated at the intersection of the grout and the bolt (see Figure 17(e)). When the shear displacement reached 1 mm, the shearing process of the bolted specimen finished as shown in Figure 17(f). There were many cracks at the joints with steeper asperity angles, and the position of infilled rock joints was reinforced by rock bolts.

3.3. Effect of Infill Thickness on Shear Characteristics. The infill thickness has a significant influence on the shear characteristics of bolted infilled rock joints.. Therefore, direct shear tests with three different infill thicknesses (2.1 mm, 2.6 mm, and 3.1 mm) were continued under three different JRC conditions (JRC 6–8, JRC 12–14, and JRC 18–20). Figure 18 shows the relationship between the shear stress and shear displacement at the infill thicknesses of 2.1 mm, 2.6 mm, and 3.1 mm under JRC 18–20. Its development trend was the same as mentioned in Section 3.1.

The simulation results with those obtained for bolted and unbolted infilled rock joints under different infill thicknesses are shown in Figure 19. The observation was that the peak shear stresses for infill thicknesses of 2.1 mm, 2.6 mm, and 3.1 mm were 13.67 MPa, 11.02 MPa, and 9.61 MPa, respectively, under bolted infilled rock joints. For the unbolted cases, the peak shear stresses for infill thicknesses of 2.1 mm, 2.6 mm, and 3.1 mm were 11.17 MPa, 10.16 MPa, and 8.82 MPa, respectively. Another observation was that the bolt could increase the peak shear stress of the infilled joint. The values of the increase in peak shear stress for infill

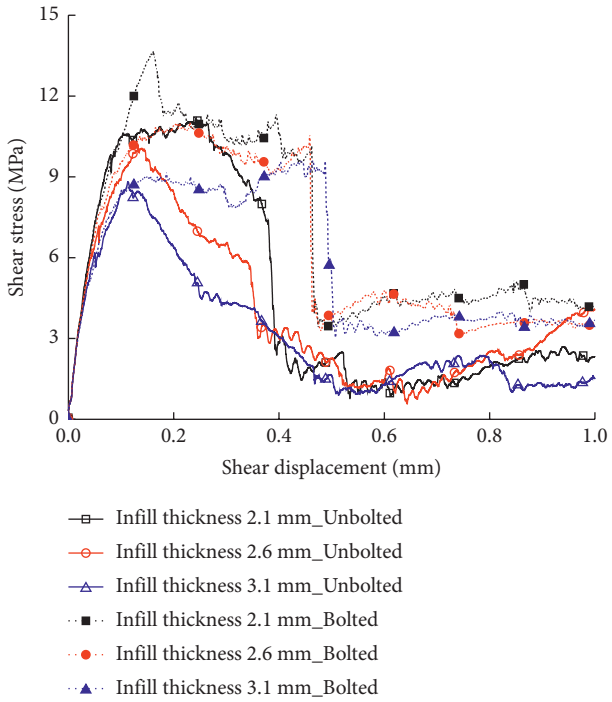

Figure 18: Relationship between shear stress and shear displacement under different infill thicknesses.

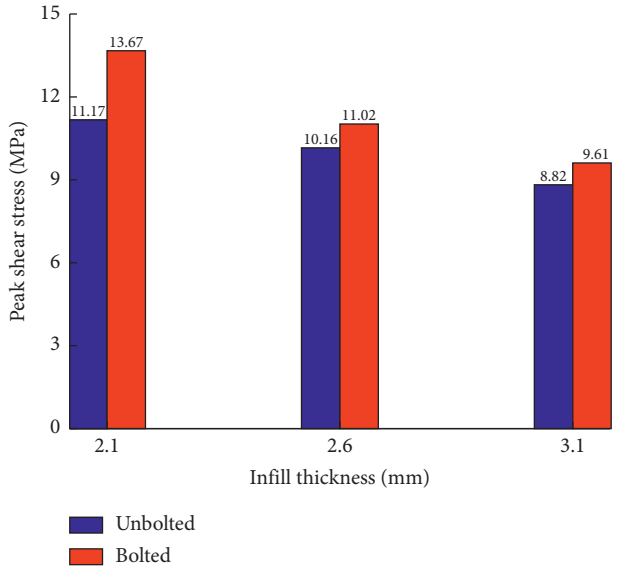

Figure 19: Relationship between peak shear stress and infill thickness.

thicknesses of 2.1 mm, 2.6 mm, and 3.1 mm were 2.50 MPa, 0.86 MPa, and 0.79 MPa, respectively.

4. The Coupling Effect of Joint Roughness and Infill Thickness on Peak Shear Stress

It can be seen from the above research results that joint roughness and infill thickness have important effects on the shear characteristics of bolted infilled rock joints. Meanwhile, we cannot ignore the fact that joint roughness and infill thickness often have a coupling influence on actual engineering. In this section, we discuss the influence of the changes of joint roughness and infill thickness on the bolted infilled rock joints and unbolted specimens. To study the coupling influence of joint roughness and infill thickness, 18 groups of tests were carried out on the bolted and unbolted specimens.

The coupling influence of joint roughness and infill thickness on the peak shear stress is shown in Figure 20. It can be seen from the figure that the peak shear stress of the bolted specimens was significantly higher than that of the unbolted specimens. When the infill thickness was constant, the peak shear stress of the unbolted and bolted specimens showed an upward trend with increasing joint roughness. When the joint roughness coefficient was constant, the peak shear stress of the unbolted and bolted samples showed a downward trend with increasing infill thickness.

As shown in Tables 3 and 4, when JRC increases gradually, the change rate of peak shear stress of unbolted sample is higher than that of bolted sample. As the infill thickness increases, this change rate increases from 2.63 to 2.80 for the unbolted joint. However, for bolted sample, when infill thickness increases, this change rate gradually decreases, from 1.45 to 1.25. The above results indicate that the unbolted samples are highly sensitive to JRC changes. The greater the infill thickness, the greater the sensitivity of unbolted samples to JRC changes.

When the infill thickness decreases from 3.1 mm to 2.1 mm, the change rate of peak shear stress decreases from 1.35 to 1.27 for unbolted sample as the JRC value increases. For bolted sample, the change rate increases from 1.22 to 1.42 with the increase of JRC value. The above results show that the value of change multiple of infill thickness is almost

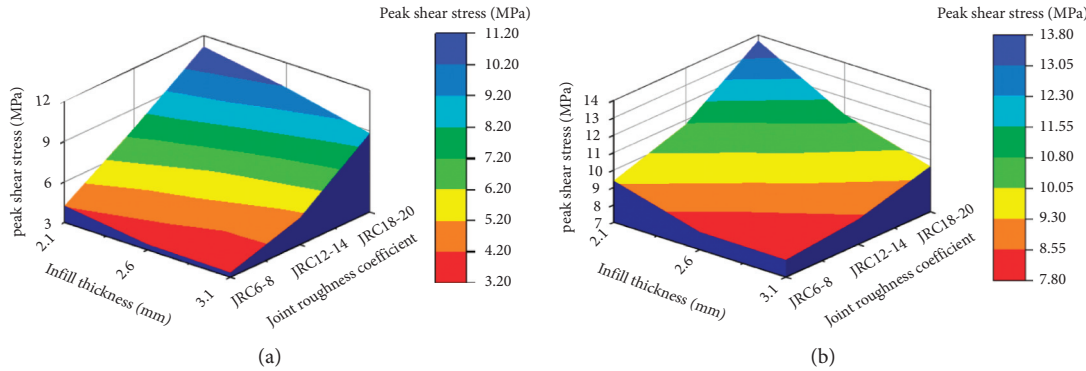

Figure 20: Relationship between peak shear stress and coupling of joint roughness and infill thickness for infilled rock joints: (a) unbolted; (b) bolted.

Table 3: Relationship between peak shear stress and coupling of joint roughness and infill thickness for unbolted infilled rock joints.

Infill thickness	JRC			Change multiple (from 6–8 to 18–20)
	6–8	12–14	18–20	
2.1 mm	4.24 MPa	7.35 MPa	11.17 MPa	2.63
2.6 mm	3.67 MPa	6.38 MPa	10.16 MPa	2.77
3.1 mm	3.15 MPa	5.78 MPa	8.82 MPa	2.80
Change multiple (from 3.1 mm to 2.1 mm)	1.35	1.27	1.27	—

Table 4: Relationship between peak shear stress and coupling of joint roughness and infill thickness for bolted infilled rock joints.

Infill thickness	JRC			Change multiple (from 6–8 to 18–20)
	6–8	12–14	18–20	
2.1 mm	9.39 MPa	10.75 MPa	13.67 MPa	1.45
2.6 mm	8.50 MPa	9.57 MPa	11.02 MPa	1.30
3.1 mm	7.69 MPa	8.44 MPa	9.61 MPa	1.25
Change multiple (from 3.1 mm to 2.1 mm)	1.22	1.27	1.42	—

the same for the two kinds of specimens, whether with bolt or not; that is, the influence degree of infill thickness on the samples is almost the same. Another finding is that for unbolted sample, the increase of JRC weakens this multiple of peak shear stress changes as the infill thickness decreases.

The reason for the above results may be that the reinforcement effect of the bolt will strengthen the meshing strength between the joint surface and the filling material. Moreover, the meshing strength is positively correlated with joint roughness and negatively correlated with filling thickness.

5. Conclusions

In this paper, a method of importing standard joint profile into PFC2D was proposed. Through a series of numerical shear tests, the shear characteristics and micro-cracks of infilled rock joints have been discussed in detail under different JRC and infill thickness conditions. The influence of bolting structure was also considered. Moreover, the coupling effect of joint roughness and infill thickness on peak shear stress was further analyzed. The specific conclusions are as follows:

(1) The numerical results revealed that rock bolts profoundly improved the shear strength of the infilled rock joints, enhanced the toughness of the joint surface, increased the number of micro-cracks, and made the dilatation more obvious. The shear stress and the normal displacement of unbolted or bolted infilled rock joints increased with increasing the joint roughness and decreasing the infill thickness. The micro-cracks increased with increasing the joint roughness and infill thickness.

(2) To study the evolution process of the stress on the bolt in the direct shear tests, five measurement circles were uniformly distributed in the rock bolt. The monitoring results show that S_{xx}, S_{xy}, and S_{yy} in the middle of the bolt are higher than those in other positions. In addition, the maximum horizontal compression stress in the middle of the bolt gradually increased with the increase of JRC.

(3) Different roughness has different effects on the number of micro-cracks in the sample. The number of total cracks and tensile cracks of the bolted and unbolted specimens increased with the increase of joint roughness coefficient, while the shear cracks remained almost the same. There were few micro-

cracks in the unbolted or bolted specimens at the beginning of the shear test. It was observed that cracks began to form around the edges of rock joints. When the shear displacement increased, the infill was completely penetrated by cracks. Then, the bolt was destroyed, and a lot of cracks were generated at the intersection of the grout and the bolt.

(4) Through the study of the coupling effect of joint roughness and infill thickness on peak shear stress, the following results were obtained. When JRC increases gradually, the change rate of peak shear stress of unbolted sample is higher than that of bolted sample. This indicated that the unbolted samples are highly sensitive to JRC changes. The greater the infill thickness, the greater the sensitivity of unbolted samples to JRC changes.

Another finding is that for unbolted specimens, the increase of JRC decreases the change multiple of peak shear stress as the filling thickness decreases. This is probably because the reinforcement effect of the bolt will strengthen the meshing strength between the joint surface and the filling material. Moreover, the meshing strength is positively correlated with joint roughness and negatively correlated with filling thickness.

Data Availability

The data can be available by contacting the corresponding author.

Conflicts of Interest

The authors declare that they have no known competing financial interests or personal relationships that could have appeared to influence the work reported in this paper.

Acknowledgments

This study has been partially funded by National Natural Science Foundation of China (No. 41907251, No. 52179098, No. 51678155), Natural Science Foundation of Fujian Province (No. 2019J05030), Postdoctoral Science Foundation of China (2019M652247), and Opening Foundation of Shandong Key Laboratory of Civil Engineering Disaster Prevention and Mitigation (CDPM2019KF04). This support is gratefully acknowledged.

References

[1] S. Q. Yang, P. F. Yin, Y. C. Zhang et al., "Failure behavior and crack evolution mechanism of a non-persistent jointed rock mass containing a circular hole," *International Journal of Rock Mechanics and Mining Sciences*, vol. 114, pp. 101–121, 2019.

[2] M. S. Asadi, V. Rasouli, and G. Barla, "A laboratory shear cell used for simulation of shear strength and asperity degradation of rough rock fractures," *Rock Mechanics and Rock Engineering*, vol. 46, no. 4, pp. 683–699, 2013.

[3] Y. Jiang, Y. Wang, P. Yan, H. Luan, and Y. Chen, "Experimental investigation on the shear properties of heterogeneous discontinuities," *Geotechnical & Geological Engineering*, vol. 37, no. 6, pp. 4959–4968, 2019.

[4] D. Huang, D. F. Cen, G. W. Ma, and R. Q. Huang, "Step-path failure of rock slopes with intermittent joints," *Landslides*, vol. 12, no. 5, pp. 911–926, 2015.

[5] V. Sarfarazi and W. Schubert, "Sliding phenomena in intermittent rock joint," *Periodica Polytechnica: Civil Engineering*, pp. 351–360, 2016.

[6] F. Meng, L. N. Y. Wong, H. Zhou, J. Yu, and G. Cheng, "Shear rate effects on the post-peak shear behaviour and acoustic emission characteristics of artificially split granite joints," *Rock Mechanics and Rock Engineering*, vol. 52, no. 7, pp. 2155–2174, 2019.

[7] Q. Z. Chen, Y. M. Liu, and S. Y. Pu, "Strength characteristics of nonpenetrating joint rock mass under different shear conditions," *Advances in Civil Engineering*, vol. 2020, Article ID 3579725, 13 pages, 2020.

[8] G. H. Zhao, L. G. Wang, N. Zhao, J. L. Yang, and X. L. Li, "Analysis of the variation of friction coefficient of sandstone joint in sliding," *Advances in Civil Engineering*, vol. 2020, Article ID 8863960, 12 pages, 2020.

[9] Z. C. Tang, Q. Z. Zhang, and J. Peng, "Effect of thermal treatment on the basic friction angle of rock joint," *Rock Mechanics and Rock Engineering*, vol. 53, no. 4, pp. 1973–1990, 2019.

[10] S. Ma, N. Aziz, J. Nemcik, and A. Mirzaghorbanali, "The effects of installation procedure on bond characteristics of fully grouted rock bolts," *Geotechnical Testing Journal*, vol. 40, no. 5, pp. 846–857, 2017.

[11] K. Spang and P. Egger, "Action of fully-grouted bolts in jointed rock and factors of influence," *Rock Mechanics and Rock Engineering*, vol. 23, no. 3, pp. 201–229, 1990.

[12] G. Grasselli, "3D Behaviour of bolted rock joints: experimental and numerical study," *International Journal of Rock Mechanics and Mining Sciences*, vol. 42, no. 1, pp. 13–24, 2005.

[13] X. Li, N. Aziz, A. Mirzaghorbanali, and J. Nemcik, "Behavior of fiber glass bolts, rock bolts and cable bolts in shear," *Rock Mechanics and Rock Engineering*, vol. 49, no. 7, pp. 2723–2735, 2016.

[14] X. Wu, Y. Jiang, B. Gong, T. Deng, and Z. Guan, "Behaviour of rock joint reinforced by energy-absorbing rock bolt under cyclic shear loading condition," *International Journal of Rock Mechanics and Mining Sciences*, vol. 110, pp. 88–96, 2018.

[15] X. Wu, Y. Jiang, G. Wang, B. Gong, Z. Guan, and T. Deng, "Performance of a new yielding rock bolt under pull and shear loading conditions," *Rock Mechanics and Rock Engineering*, vol. 52, no. 9, pp. 3401–3412, 2019.

[16] H. Lin, Z. Xiong, T. Liu, R. Cao, and P. Cao, "Numerical simulations of the effect of bolt inclination on the shear strength of rock joints," *International Journal of Rock Mechanics and Mining Sciences*, vol. 66, pp. 49–56, 2014.

[17] L. Li, P. C. Hagan, S. Saydam, B. Hebblewhite, and Y. Li, "Parametric study of rockbolt shear behaviour by double shear test," *Rock Mechanics and Rock Engineering*, vol. 49, no. 12, pp. 4787–4797, 2016.

[18] A. Mirzaghorbanali, H. Rasekh, N. Aziz, G. Yang, S. Khaleghparast, and J. Nemcik, "Shear strength properties of cable bolts using a new double shear instrument, experimental study, and numerical simulation," *Tunnelling and Underground Space Technology*, vol. 70, pp. 240–253, 2017.

[19] H. Jalalifar and N. Aziz, "Experimental and 3D numerical simulation of reinforced shear joints," *Rock Mechanics and Rock Engineering*, vol. 43, no. 1, pp. 95–103, 2010.

[20] H. Lin, P.-H. Sun, and Y. Chen, "Shear strength of flat joint considering influencing area of bolts," *Advances in Civil Engineering*, vol. 2020, Article ID 8878432, 12 pages, 2020.

[21] M. Saadat and A. Taheri, "Effect of contributing parameters on the behaviour of a bolted rock joint subjected to combined pull-and-shear loading: a DEM approach," *Rock Mechanics and Rock Engineering*, vol. 53, no. 1, pp. 383–409, 2020.

[22] J. Shang, Y. Yokota, Z. Zhao, and W. Dang, "DEM simulation of mortar-bolt interface behaviour subjected to shearing," *Construction and Building Materials*, vol. 185, pp. 120–137, 2018.

[23] Q.-Q. Ren, J.-Q. Feng, J. Ma, and H. Du, "Filling provenance in fracture cavity formation within aksu area, tarim basin, NW China: indicators from major and trace element, carbon-oxygen, and strontium isotope compositions," *Lithosphere*, vol. 2021, Article ID 5559457, 2021.

[24] L. Gong, A. Heitor, and B. Indraratna, "An approach to measure infill matric suction of irregular infilled rock joints under constant normal stiffness shearing," *Journal of Rock Mechanics and Geotechnical Engineering*, vol. 10, no. 4, pp. 653–660, 2018.

[25] G. Han, H. Jing, Y. Jiang, R. Liu, and J. Wu, "Effect of cyclic loading on the shear behaviours of both unfilled and infilled rough rock joints under constant normal stiffness conditions," *Rock Mechanics and Rock Engineering*, vol. 53, no. 1, pp. 31–57, 2020.

[26] Q. S. Liu, G. F. Lei, and X. X. Peng, "Study on shear mechanical properties of sandstone, marble and granite after anchoring," *Chinese Journal of Rock Mechanics and Engineering*, vol. 37, no. S2, pp. 4007–4015, 2018.

[27] N. Barton and V. Choubey, "The shear strength of rock joints in theory and practice," *Rock Mechanics*, vol. 10, no. 1-2, pp. 1–54, 1977.

[28] X. Wu, Y. Jiang, and B. Li, "Influence of joint roughness on the shear behaviour of fully encapsulated rock bolt," *Rock Mechanics and Rock Engineering*, vol. 51, no. 3, pp. 953–959, 2018.

[29] M. Saadat and A. Taheri, "A numerical study to investigate the influence of surface roughness and boundary condition on the shear behaviour of rock joints," *Bulletin of Engineering Geology and the Environment*, vol. 79, pp. 1–16, 2020.